International Journal of Mathematical Archive-6(1), 2014, 10-19
Available online through www.ijma.info ISSN 2229 – 5046

ANALYTICAL STUDY ON INFLUENCE OF HEAT SOURCE / SINK ON TEMPERATURE DISTRIBUTION IN MHD BOUNDARY LAYER FLOW OVER A PERMEABLE SHRINKING SHEET EMBEDDED WITH POROUS MEDIUM

Chandaneswar Midya*

Department of Mathematics,
Ghatal Rabindra Satabarsiki Mahavidyalaya, Paschim Medinipur, West Bengal - 721212, India.

(Received On: 17-12-14; Revised & Accepted On: 08-01-15)

ABSTRACT

In this paper, effects of radiation and heat source/sink on heat transfer in hydromagnetic boundary layer flow over a linearly shrinking permeable surface embedded with porous medium are studied analytically. The governing boundary layer equations for fluid flow and energy are reduced into ordinary differential equations by means of a similarity transformations. The solution of momentum equation is used in solving reduced energy equation exactly for power-law surface temperature boundary condition. The skin friction coefficient increases for increasing suction, magnetic field and porosity parameter. It is found that in heat sink case, dual temperature profiles exist corresponding to dual solutions of momentum equation. But, in heat source case dual temperature corresponding to dual solutions of flow field exist only if certain condition is satisfied. In heat sink case, dual solutions of boundary layer temperature shows different feature for magnetic field and porosity parameter. Thermal boundary layer decreases for increasing values of radiation parameter, Prandtl number and suction parameter in both heat source and heat sink cases. In heat case and for some positive power index in temperature boundary conditions, one of the dual solutions in temperature field becomes negative.

Keywords: *Permeable shrinking sheet, MHD, Porous medium, Boundary layer flow, Radiation, Heat Source/sink, Analytical solution.*

1. INTRODUCTION

Energy saving is a hot topic in today's world because of the fact that fuel is becoming more and more valuable day by day. Boundary layer heat transfer in an incompressible viscous fluid flow over a shrinking sheet may show a path to way out from these crucial crisis. The fact behind this is that flow over a shrinking sheet is a new type of flow and thermal boundary layer thickness in this type of flow is very large compared to the same problem of flows over a stretching sheet. Because of the larger thickness in thermal boundary layer, heat can be maintained up to a very long range near the shrinking slot. This phenomenon can be useful in industry where liquid temperature is to maintain in a very long region near the wall. The pioneering work in the area of flow over a shrinking sheet was reported by Wang [1]. Later, Miklavcic and Wang [2] derived an analytical solution for steady viscous hydrodynamic flow over a permeable shrinking sheet. Muhaimin *et al.* [3] presented numerically the effects of heat and mass transfer on MHD boundary layer flow over a shrinking sheet in the presence of suction. Nadeem and Hussain [4] used homotopy analysis method to study the viscous flow on a nonlinear porous shrinking sheet. Fang and Zhang [5] solved the Full N-S equation analytically for two dimensional MHD viscous flow due to a shrinking sheet. Fang and Zhang [6] first studied the heat transfer characteristics of the flow over a shrinking sheet analytically. Later, Noor et al. [7] studied the MHD viscous flow due to shrinking sheet using Adomian decomposition Method (ADM) and they obtained a series solution. Ali et al. [8] studied magnetohydrodynamics viscous flow and heat transfer induced by a permeable shrinking sheet with prescribed surface heat flux. Effect of chemical reaction, heat and mass transfer on nonlinear boundary layer past a porous shrinking sheet in the presence of suction was studied numerically by Muhaimin *et al.* [9]. Midya [10] analytically studied the magnetohydrodynamic viscous flow and heat transfer over a linearly shrinking permeable sheet without heat source/sink. Most recently, Midya [11] obtained a closed form analytical solution for the distribution of heat in a boundary layer flow over a permeable shrinking sheet with heat source/sink. Bhattacharyya [12] studied numerically the effects of heat source/sink on unsteady MHD flow and heat transfer over a shrinking sheet with mass

*Corresponding Author: Chandaneswar Midya**

suction and in the absence of porous medium and radiation. Bhattacharyya [13] also investigated effects of heat source/sink on unsteady MHD flow and heat transfer over a shrinking sheet with mass suction and in the absence of porous medium numerically. Their study did not find the dual temperature profile for heat sink and necessary condition required for having solutions of thermal boundary layer in heat source case. For small values of magnetic field or suction or higher values of injection which generate larger thickness in thermal boundary layer in comparison to large magnetic field or suction or small values of injection on flows over a shrinking sheet, solving these problems through numerical is either erroneous or sometimes become difficult to capture full physics of the problem. For is reason, most of the authors use higher suction values or higher magnetic field in order to reduce the thickness of thermal boundary layer which in turn help to compute the problem numerically. On the contrary use of analytical methods removes all the above mentioned hazards. In this paper we investigate analytically the effects of heat source / sink on heat transfer in an electrically conducting viscous incompressible fluid flow over a linearly shrinking permeable sheet embedded with porous medium and in the presence of magnetic field and heat radiation. We study temperature distributions for varying values of various controlling parameters along with dual temperatures in heat sink case.

2. MATHEMATICAL FORMULATION

Consider the flow of an electrically conducting incompressible fluid over a permeable flat sheet embedded with porous medium. Let x-axis and y-axis be taken respectively along and perpendicular to the sheet and the flow is confined to y > 0. Two equal and opposite forces are applied opposite to the x -axis so that the wall is shrinked keeping the origin fixed. A magnetic induction B_0 is applied perpendicular to the shrinking surface. The shrinking sheet velocity is proportional to the distance i.e. u_w = -ax, (a > 0). Neglecting induced magnetic field, the boundary layer equations for steady two-dimensional flow and energy can be written in usual notations as

$$\frac{\partial u}{\partial x}+\frac{\partial v}{\partial y}=0, \tag{1}$$

$$u\frac{\partial u}{\partial x}+v\frac{\partial u}{\partial y}=\nu\frac{\partial^2 u}{\partial y^2}-\frac{\sigma B_0^2}{\rho}u-\frac{\nu}{k_p}u, \tag{2}$$

$$u\frac{\partial T}{\partial x}+v\frac{\partial T}{\partial y}=\frac{\kappa}{\rho c_p}\frac{\partial^2 T}{\partial y^2}-\frac{1}{\rho c_p}\frac{\partial q_r}{\partial y}+\frac{Q}{\rho c_p}(T-T_\infty), \tag{3}$$

where u and v are the components of velocity respectively in the x and y directions, T is the temperature, T_∞ is the temperature far from the sheet, ρ is the fluid density (assumed constant), σ is the electrical conductivity of the fluid, ν (= μ/ρ) is the coefficient of fluid viscosity, κ is the thermal conductivity, q_r is the radiative heat flux, Q is the volumetric rate of internal heat generation / absorption and k_p is the parameter corresponding to porous medium. The negative values of Q corresponds to heat absorption and positive values of Q indicate heat generation.

The boundary conditions for the velocity components and temperature are given by

$$u=-ax,\ \ v=v_w,\ \ T=T_w=T_\infty+Ax^p \quad at\ y=0 \tag{4}$$

and

$$u\longrightarrow 0,\ \ v\longrightarrow 0,\ \ T\longrightarrow T_\infty \quad at\ y\longrightarrow\infty, \tag{5}$$

where T_w is the wall temperature.

Now, using Rosseland's approximation for radiation, q_r can be expressed as $q_r=-(4\sigma^*/3k_1)\,\partial T^4/\partial y$, where σ^* is the Stefan-Boltzmann constant, k_1 is the absorption coefficient (see Brewster [14]). It is assumed that the temperature variation within the flow is such that T^4 may be expanded in a Taylor's series. Expanding T^4 about T_∞ and neglecting higher order terms, we have $T^4=4T_\infty^3T-3T_\infty^4$.

Therefore, Eq. (3) reduces to

$$u\frac{\partial T}{\partial x}+v\frac{\partial T}{\partial y}=\frac{\kappa}{\rho c_p}\frac{\partial^2 T}{\partial y^2}+\frac{16\sigma^*}{3k_1}\frac{T_\infty^3}{\rho c_p}\frac{\partial^2 T}{\partial y^2}+\frac{Q}{\rho c_p}(T-T_\infty) \tag{6}$$

3. SOLUTION OF THE PROBLEM

Let us take

$$u=axf'(\eta),\ \ v=-\sqrt{a\nu}f(\eta),\ \ \eta=y\sqrt{\frac{a}{\nu}} \tag{7}$$

as the self-similar solutions of the equations (1), (2) and (6) along with the boundary conditions (4) and (5). Here f is the dimensionless stream function and η is the similarity variable.

Substitution of these leads Eq. (2) into

$$\frac{d^3f}{d\eta^3}+f\frac{d^2f}{d\eta^2}-\left(\frac{df}{d\eta}\right)^2-(M^2+\lambda)\frac{df}{d\eta}=0, \tag{8}$$

where $M = \sqrt{\sigma B_0^2/(a\rho)}$ is the magnetic interaction parameter and $\lambda = \frac{\mu}{ak_p}$ is the porosity parameter.

Using Eqs. (7), the boundary conditions for flow reduce to

$$f'(0) = -1,\ \ f(0) = s,\ \ and\ \ f'(\infty) = 0, \tag{9}$$

where $s = -v_w/\sqrt{av}$ is a non-dimensional constant with s > 0 for suction and s < 0 corresponds to injection.

The energy equation (Eq. (6)) also reduces to

$$\frac{d^2\theta}{d\eta^2} + DPrf\frac{d\theta}{d\eta} + DPr\left(\gamma - p\frac{df}{d\eta}\right)\theta = 0, \tag{10}$$

where $\theta(\eta) = \frac{T-T_\infty}{T_w-T_\infty}, Pr = \frac{\mu c_p}{\kappa} and\ \gamma = \frac{Q}{\rho c_p a}$ respectively denote non-dimensional temperature, Prandtl number and heat source / sink parameter. The negative values of γ corresponds to heat sink and positive values of γ indicate heat source. D = 3R/(3R+4), where R is the thermal radiation parameter given by $R = \kappa k_1/4\sigma^* T_\infty^3$.

The boundary conditions for temperature then become

$$\theta(0) = 1,\ \ and\ \ \theta(\infty) = 0. \tag{11}$$

Now, Equation (8) along with the boundary conditions admits an analytical solution (see Fang and Zhang [5]) given by

$$f(\eta) = s - \frac{1}{\alpha}(1 - e^{-\alpha\eta}), \tag{12}$$

where α is the positive real root of the equation

$$t^2 - st + 1 - (M^2 + \lambda) = 0. \tag{13}$$

It is, therefore, seen that there are two exponential solutions for any s > 0, $0 < M^2 + \lambda < 1$ with $s^2 > 4[1-(M^2 + \lambda)]$ and there is one solution for the cases (i) s > 0 , $0 < M^2 + \lambda < 1$with $s^2 = 4[1-(M^2 + \lambda)]$, (ii) s > 0, $M^2 + \lambda = 1$ and (iii) $-\infty < s < +\infty$, $(M^2 + \lambda) > 1$. For all other cases, the roots of the equation (8) become either zero or negative and hence no exponential solution exist.

The non-dimensional horizontal velocity component is given by

$$f'(\eta) = -e^{-\alpha\eta} \tag{14}$$

The shear stress at the wall is denoted by τ_w and is defined as

$$\tau_w = \mu(\partial u/\partial y)_{y=0} = \mu ax\sqrt{\frac{a}{\nu}}f''(0) = \mu ax\sqrt{\frac{a}{\nu}}\,\alpha \tag{15}$$

The skin friction coefficient C_f at the wall is obtained as

$$C_f = \frac{\tau_w}{\left(\mu ax\sqrt{\frac{a}{\nu}}\right)} = f''(0) = \alpha \tag{16}$$

Now, substituting the solution for the momentum transport, the above temperature Eq. (10) reduces to

$$\frac{d^2\theta}{d\eta^2} + DPr\{s - \frac{1}{\alpha}(1 - e^{-\alpha\eta})\}\frac{d\theta}{d\eta} + DPr(\gamma + pe^{-\alpha\eta})\theta = 0 \tag{17}$$

Now, substituting $\frac{DPr}{\alpha^2}e^{-\alpha\eta} = \xi$, the above equation transforms into

$$\xi\frac{d^2\theta}{d\xi^2} + (1 - DPr\beta - \xi)\frac{d\theta}{d\xi} + \left(p + \frac{DPr\gamma}{\alpha^2\xi}\right)\theta = 0, \tag{18}$$

where $\beta = \frac{1}{\alpha}\left(s - \frac{1}{\alpha}\right)$.

The boundary conditions (11) then become

$$\theta\left(\frac{DPr}{\alpha^2}\right) = 1,\ \ and\ \ \theta(0) = 0 \tag{19}$$

Now, we transform the above equation (18) into confluent hypergeometric equation and obtain the solution (see Abramowitz and Stegun [15]) given by

$$\theta(\xi) = (\alpha^2\xi/DPr)^\delta\,\Phi(\delta - p, 1 + b_0, \xi)/\Phi(\delta - p, 1 + b_0, DPr/\alpha^2), \tag{20}$$

where $\delta = (b_0 + a_0)/2,\ a_0 = DPr\beta, b_0 = \sqrt{a_0^2 - \frac{4a_0\gamma}{\alpha^2\beta}}$ and $\boldsymbol{\Phi}(a', b', x)$ is the confluent hypergeometric function of the first kind or Kummer function.

Now, when $\gamma < 0$ i.e. for hear sink case, we always have real b_0 and hence dual temperature profile exist for dual positive solutions for α and single temperature exists for single positive value of α. But when $\gamma > 0$ i.e. for heat source case, we will get real non-zero b_0 only when $a_0^2 - \frac{4a_0\gamma}{\alpha^2\beta} > 0$ i.e. $DPr\alpha^2\beta^2 > 4\gamma$. Therefore, in this case temperature profile can be obtained if the above condition is satisfied along with positive solutions of momentum equation.

In terms of η,

$$\theta(\eta) = e^{-\alpha\delta\eta}\, \Phi(\delta - p, 1 + b_0, DPre^{-\alpha\eta}/\alpha^2)/\Phi(\delta - p, 1 + b_0, DPr/\alpha^2). \quad (23)$$

The dimensionless wall temperature gradient $\theta'(0)$ is obtained as

$$\theta'(0) = -\alpha\delta - \frac{DPr}{\alpha}\left(\frac{\delta - p}{1 + b_0}\right)\frac{\Phi(1+\delta-p, 2+b_0, DPr/\alpha^2)}{\Phi(\delta-p, 1+b_0, DPr/\alpha^2)}. \quad (24)$$

4. RESULTS AND DISCUSSION

We compute the skin friction coefficient $f''(0)$ for several values of suction , magnetic field and porosity parameters and the results are displayed in Table 1. It is seen that skin friction increases for increasing values of s, M and λ. It should be noted that only one solution exists for the values of the flow parameters used here.

Table 1. Skin friction coefficient $f''(0)$ for several values of s, M and λ

s	M	λ	$f''(0)$	s	M	λ	$f''(0)$	s	M	λ	$f''(0)$
1	$\sqrt{2}$	0	1.61803	2	1	0	2	2	1	0	2
2	$\sqrt{2}$	0	2.41421	2	$\sqrt{2}$	0	2.41421	2	1	0.2	2.09545
3	$\sqrt{2}$	0	3.30278	2	2	0	3	2	1	0.5	2.22474

Next, variations of $-\theta'(0)$ are shown in Table 2 for various values of suction parameter s, radiation parameter R and heat source/sink parameter γ when M = 1, λ = 0.2, p = 0, Pr = 1. It follows from the table that $-\theta'(0)$ increases for increasing suction and radiation parameter whereas it decreases for increasing γ from negative values to positive value. It should be noted that only one solution exists for the values of the parameters used in Table 2.

Table 2. Variations of $-\theta'(0)$ when M = 1, λ = 0.2, p = 0, Pr = 1

s	R	γ	$-\theta'(0)$	s	R	γ	$-\theta'(0)$	s	R	γ	$-\theta'(0)$
1	1	-0.5	0.58803	2	1	-0.5	0.950468	2	0.5	-0.5	0.662781
2	1	-0.5	0.950468	2	1	0	0.689069	2	1	-0.5	0.950468
3	1	-0.5	1.35028	2	1	0.2	0.492335	2	1.5	-0.5	1.1338

It is already seen that two exponential solutions for the momentum equation exist corresponding to two positive root of the Equation (13) when s > 0, $0 < M^2 + \lambda < 1$ and $s^2 > 4[1-(M^2 + \lambda)$. Let us recognize the positive root $t = (s + \sqrt{s^2 - 4\{1 - (M^2 + \lambda)\}})/2$ as first solution and the positive root $t = (s - \sqrt{s^2 - 4\{1 - (M^2 + \lambda)\}})/2$ as second solution. We now discuss heat sink and heat source cases separately.

CASE-I: TEMPERATURE DISTRIBUTIONS IN HEAT SINK

We have noticed that, in heat sink case dual temperature profiles exist corresponding to dual solutions of momentum equation. The temperature profiles corresponding to first solution and second solution for different values of the radiation parameter R (R = 0.5, 1.0, 1.5) are depicted in Figure 1(a) and Figure 1(b) respectively when s = 2, M = 0.6, Pr = 1, γ = - 1, $\lambda = 0.1$ and p = 1. The temperature within the fluid corresponding to both solutions are seen to be reduced throughout the boundary layer for increasing values of radiation parameter R. It is also observed that the boundary layer thickness for second solution is much higher than that of the first solution for fixed values of η near the shrinking sheet. At a large distance from the sheet the temperature takes its limiting value T_∞.

The temperature profiles corresponding to first solutions and second solutions for different values of the Prandtl number Pr (Pr = 0.5, 1.0, 1.5) are displayed in Figure 2(a) and Figure 2(b) respectively for s = 2, M = 0.9, R = 0.7, γ = - 1.5, $\lambda = 0.1$ and p = 1. The temperature within the fluid corresponding to both the solutions reduce throughout the boundary layer for increasing values of Prandtl number Pr. The increase of Prandtl number means slow rate of thermal diffusion. Because of reduced thermal conductivity, there would be a thinning of the thermal boundary layer and this leads to the decrease in the temperature.

Figure 3(a) and Figure 3(b) respectively present temperature distributions corresponding to first solutions and second solutions for different values of the suction parameter s (s = 0.5, 1.0, 1.5) when R = 0.7, M = 0.9, Pr = 1, γ = - 1, $\lambda = 0.1$ and p = 1. We notice that the effect of suction parameter s is to decrease the temperature in the boundary layer

for both the solutions. Due to suction at the sheet hot fluid particles are sucked from the flow field and hence temperature within the boundary layer decrease.

We shall now concentrate on the temperature distributions corresponding to first and second solutions for varying values of magnetic parameter M when other parameters are s = 2, R = 0.7, Pr = 1, γ = - 1, $\lambda = 0.1$ and p = 1 and these are shown in Figure 4(a) and Figure 4(b) respectively. It is interesting to note that temperature within the boundary layer decreases for the increase in magnetic field for the first solution whereas different picture is seen for second solution. In second solution temperature increases for increasing M.

The temperature profiles for different values of heat sink parameter γ are depicted in Figure 5(a) and Figure 5(b) respectively corresponding to first solution and second solution when s = 2, M = 0.9, Pr = 1, R = 0.7, $\lambda = 0.1$ and p = 1. The figure reveals that the temperature within the fluid decreases for the increasing values of heat sink parameter. This fact is usual because the heat energy is absorbed in this case. Also, it is noteworthy that the boundary layer thickness for second solution is much higher than that of the first solution.

Figure 6(a) and Figure 6(b) represents respectively the temperature distributions corresponding to first solution and second solution for various values of power index p (p = 0, 1, 2) with s = 2, M = 0.9, Pr = 1, γ = - 1, $\lambda = 0.1$ and R = 0.7. It is noticed from the figure that the temperature within the fluid for first solutions increase for the increasing values of power index p from 0 to 2. But, for second solution, the increase in temperature is rapid compared to the first solution for increasing p and for p = 2 temperature profile becomes negative.

The variations of temperature within the boundary layer are shown in Figure 7(a) and 7(b) for first and second solution respectively when values of the other parameters are M = 0.6, s = 2, R = 0.7, Pr = 1, γ = - 1, and p = 1. It is reflected from the figure 7(a) that temperature is seen to be decrease for increasing porosity parameter λ. But for second solution, the fact is different. Temperature increases here for increasing λ as is observed in figure 7(b).

CASE-II: TEMPERATURE DISTRIBUTIONS IN HEAT SOURCE

Let us now concentrate on the heat source case. It is already seen that in heat source case, dual temperature distribution corresponding to two exponential solutions in the flow field, exist if $DPr\alpha^2\beta^2 > 4\gamma$ is satisfied. From the equation $t^2 - st + 1 - (M^2 + \lambda) = 0$, it is seen that sum of the roots is s. Therefore, for dual positive solutions of the momentum field, if one root is large, the other root α becomes small. As a result, for small values (second solution) of α and physically valid values of other parameters, the above condition $DPr\alpha^2\beta^2 > 4\gamma$ is rarely satisfied. Thus, we study temperature distributions for first solution only in heat source case.

First of all, we discuss the effects of radiation parameter R on the temperature profiles for first solution (see Figure 8) for s = 3, M = 0.5, Pr = 1, $\gamma = 0.1$, $\lambda = 0.1$ and p = 1. It is seen that increase in radiation parameter R results decrease in temperature within the boundary layer. This can be explained by the fact that the increase of radiation parameter R implies the release of heat energy from the flow region by means of radiation and thereby temperature is decreased within the boundary layer.

The influence of Prandtl number Pr on the temperature profiles for first solution is presented in Figure 9 for s = 3, M = 0.5, R = 0.7, γ = 0.1, $\lambda = 0.1$ and p = 1. It is observed that increase in Prandtl number is to decrease in temperature throughout the boundary layer. Actually, the increase of Prandtl number means slow rate of thermal diffusion. Because of reduced thermal conductivity, there would be a thinning of the thermal boundary layer and this leads to decrease temperature in the flow field.

The temperature profiles for various values of suction parameter s are drawn in Figure 10 for fixed R = 0.7, M = 0.9, Pr = 1, γ = 0.1, $\lambda = 0.1$ and p = 1 (in case of first solution). It is noticed from the figure that the value of temperature at a particular η reduces with increasing values of suction parameter s. Due to increase in the suction parameter s, the velocity boundary layer thickness becomes thinner and thinner and consequently decrease temperature within the fluid.

We shall now concentrate on the temperature distribution for different values of magnetic field M corresponding to first solution when s = 2, R = 0.7, Pr = 1, γ = 0.1, $\lambda = 0.1$ and p = 1 and this is depicted in Figure 11. It is seen that the increase in magnetic field results decrease in temperature throughout the boundary layer.

The temperature field for different values of heat source parameters γ is depicted in Figure 12 for s = 3, R = 0.7, Pr = 1, M = 0.5, $\lambda = 0.1$ and p = 1. It can be inferred from the figure that the dimensionless temperature increases for increasing values of heat source parameters. This is obvious, because internal heat energy emission results increase in heat transfer close to the shrinking sheet.

Now, we shall draw our attention to the effects of temperature distribution when the initial temperature is varied over the sheet. The temperature profiles for different values of power-law index p are plotted in Figure 13 for s = 3, M = 0.5, Pr = 1, γ = 0.1, $\lambda = 0.1$ and R = 0.7. It is observed from the figure that the temperature increases very slowly with the increase of power-law index p.

Finally, Figure 14 presents the effects of porosity parameter λ on thermal boundary layer for first solution when M = 0.6, s = 2, R = 0.7, Pr = 1, γ = 0.1, and p = 1. The figure displays the decrease in thermal boundary layer for the increase in porosity parameter.

5. CONCLUSIONS

Heat transfer in MHD viscous fluid flow over a linearly shrinking permeable surface embedded with porous medium is investigated analytically taking into account heat radiation and heat sink / source. The exact analytical solution of the boundary layer equation for fluid flow leads to analytical solution of boundary layer energy equation subject to power-law surface temperature boundary conditions. Dual temperature profiles for heat sink are obtained for any s > 0 and $0 < M^2 + \lambda < 1$ with $s^2 > 4[1 - (M^2 + \lambda)]$. In heat source case, dual temperature can only be found for $DPr\alpha^2\beta^2 > 4\gamma$ along with above conditions for heat sink case. Thermal boundary layer decreases for increasing values of radiation parameter, Prandtl number and suction parameter in both heat source and heat sink cases. For some positive power index, negative non-dimensional temperature values are sometimes found to exist corresponding to second solutions in heat sink case.

REFERENCES

1. Wang C. Y., Liquid film on an unsteady stretching sheet, Quart. Appl. Math., 48 (1990) 601-610.
2. Miklavcic M. and Wang C. Y., Viscous flow due to a shrinking sheet, Quart Appl. Math., 64(2) (2006) 283-290.
3. Muhaimin, Kandasamy R, Khamis AB. Effects of heat and mass transfer on nonlinear MHD boundary layer flow over a shrinking sheet in the presence of suction. *Appl. Math. and Mech. (English Edition*), 29(10) (2008) 1309-1317.
4. Nadeem S, Hussain A. MHD flow of a viscous fluid on a nonlinear porous shrinking sheet with homotopy analysis method. *Appl. Math. Mech. (Engl. Ed*.), 30(12) (2009) 1569-1578.
5. Fang T, Zhang J. Closed form exact solutions of MHD viscous flow over a shrinking sheet. Commun. in *Nonlinear Sc. and Numer. Simul*., 14(7) (2009) 2853-2857.
6. Fang T, Zhang J., Thermal boundary layer over a shrinking sheet : an analytical solution, Acta Mech, 209, (2010), 325-343.
7. Noor N F M, Kechilb S A, Hashimc I. Simple non-perturbative solution for MHD viscous flow due to a shrinking sheet. *Commun. in Nonlinear Sc. and Numer. Simul.* , 15(2) (2010) 144-148.
8. Ali F. M., Nazar R. and Arifin N. M., MHD viscous flow and heat transfer induced by a permeable shrinking sheet with prescribed surface heat flux, WSEAS Trans on Math, 9(5) (2010) 365-375.
9. Muhaimin, R. Kandasamy, I. Hashim and A. B. Khamis, On the effect of chemical reaction, heat and mass transfer on nonlinear MHD boundary layer past a porous shrinking sheet with suction, Theoretical and Applied Mechanics, 36(2) (2009) 101-116.
10. Midya C. Hydromagnetic boundary layer flow and heat transfer over a linearly shrinking permeable surface. *Int. J. of Appl. Math. and Mech*., 8(3) (2012) 57-68.
11. Midya C., Exact Solutions of Heat Transfer in Boundary Layer Flow over a Permeable Shrinking Sheet in the Presence of Radiation and Heat Source / Sink, Sci. Res. Lib. : J. Engg. Tech. Res., 2(5) (2014) 447-56.
12. Bhattacharyya K., Effects of heat source/sink on MHD flow and heat transfer over a shrinking sheet with mass suction, Chem. Engg. Res. Bulletin 15 (2011) 12-17.
13. Bhattacharyya K., Effects of radiation and heat source/sink on unsteady MHD boundary layer flow and heat transfer over a shrinking sheet with suction/injection, Front. Chem. Sci. Eng. 2011, 5(3): 376-384.
14. Brewster, Thermal Radiative Transfer Properties, John Wiley and Sons, (1972).
15. Abramowitz M., Stegun I. A., Handbook of Mathematical Functions, Dover Publications, New York, (1972).

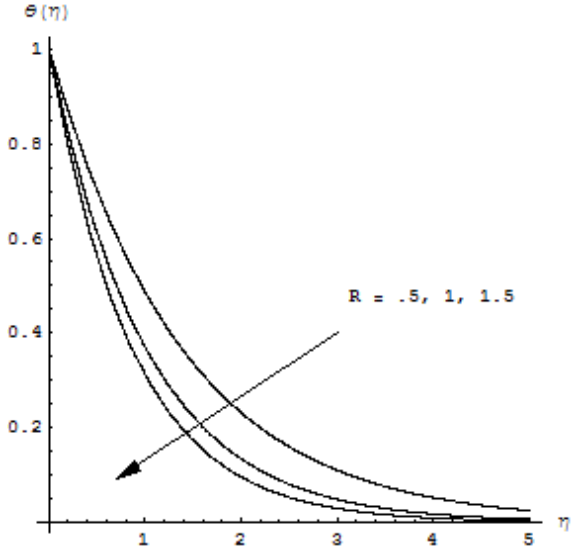

Figure 1(a): Variation of temperature corresponding to first solution for several values of R when s = 2, M = 0.6, Pr = 1, γ = - 1, $\lambda = 0.1$ and p = 1.

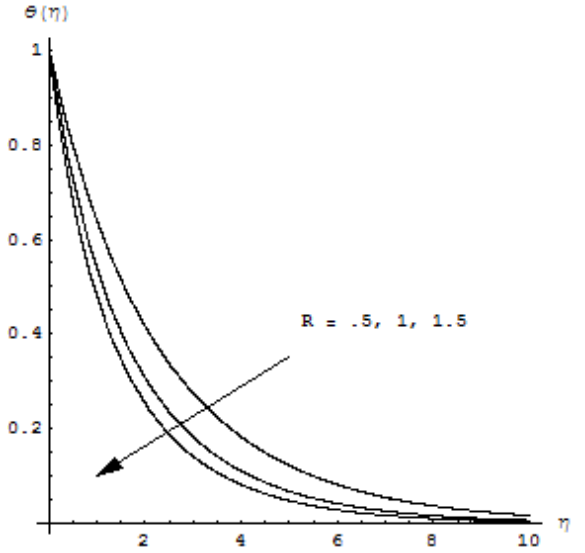

Figure 1(b): Temperature profiles corresponding to second solution for several values of R when s = 2, M = 0.6, Pr = 1, γ = - 1, $\lambda = 0.1$ and p = 1.

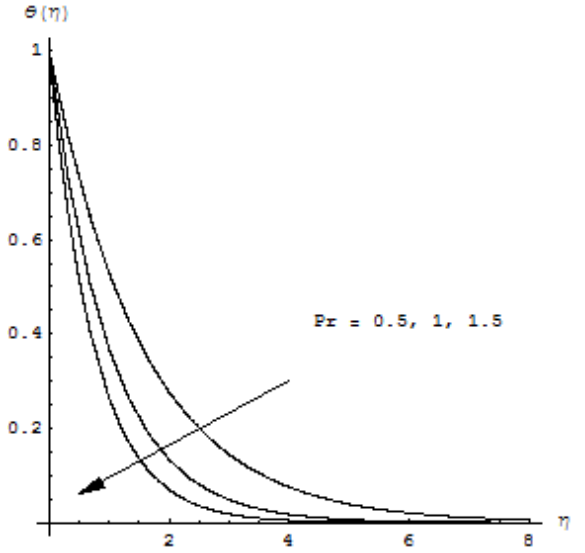

Figure 2(a): Variation of temperature corresponding to first solution for several values of Pr with s = 2, M = 0.9, R = 0.7, γ = - 1.5, $\lambda = 0.1$ and p = 1.

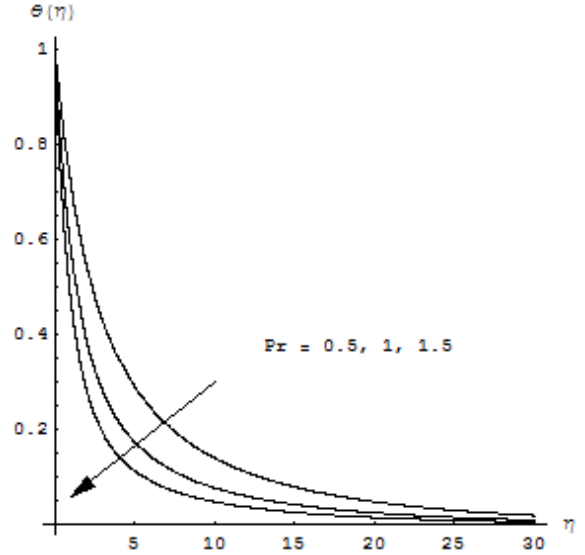

Figure 2(b): Temperature profiles corresponding to second solution for several values of Pr with s = 2, M = 0.9, R = 0.7, γ = - 1.5, $\lambda = 0.1$ and p = 1.

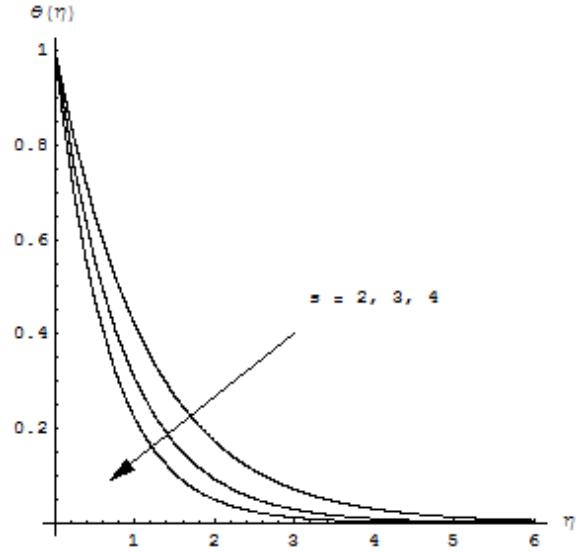

Figure 3(a): Variation of temperature corresponding to first solution for several values of s with R = 0.7, M = 0.9, Pr = 1, γ = - 1, $\lambda = 0.1$ and p = 1.

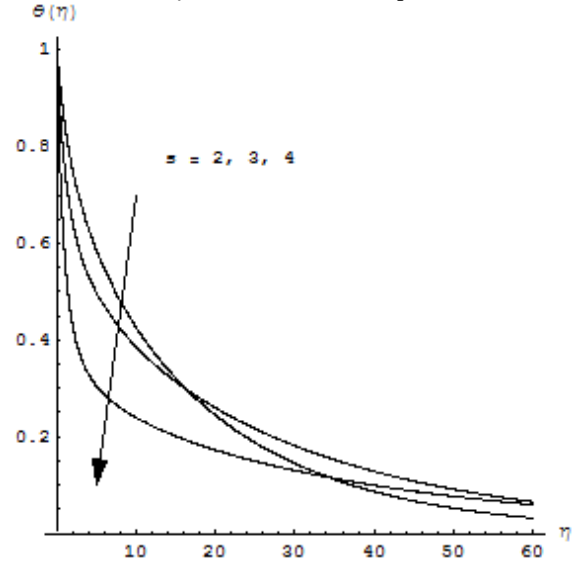

Figure 3(b): Temperature profiles corresponding to second solution for several values of s when R = 0.7, M = 0.9, Pr = 1, γ = - 1, $\lambda = 0.1$ and p = 1.

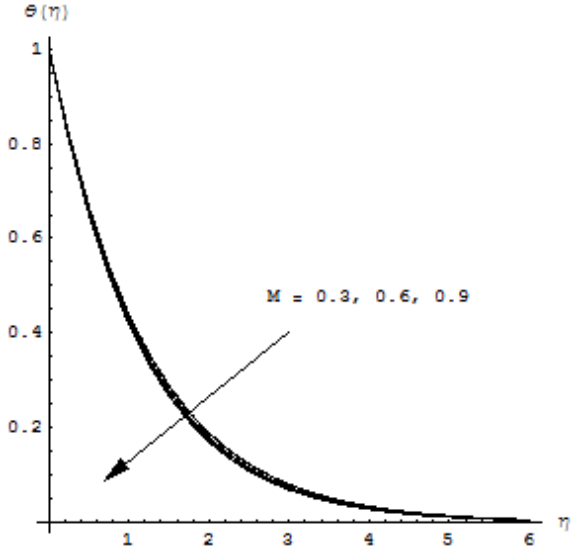

Figure 4(a): Variation of temperature corresponding to first solution for several values of M with s = 2, R = 0.7, Pr = 1, γ = - 1, $\lambda = 0.1$ and p = 1.

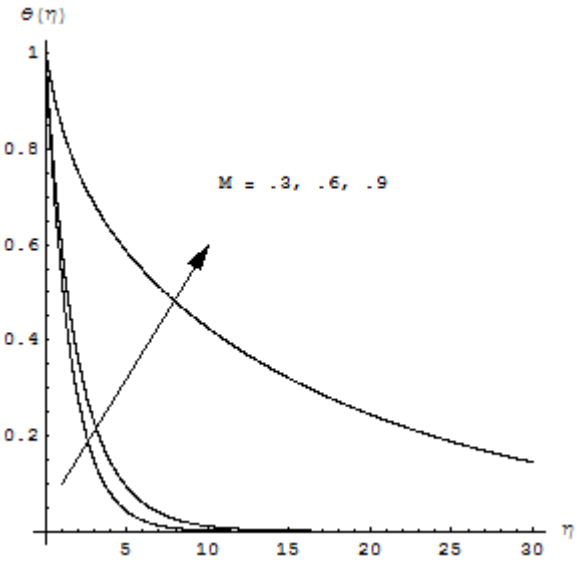

Figure 4(b): Temperature profiles corresponding to second solution for several values of M when s = 2, R = 0.7, Pr = 1, γ = - 1, $\lambda = 0.1$ and p = 1.

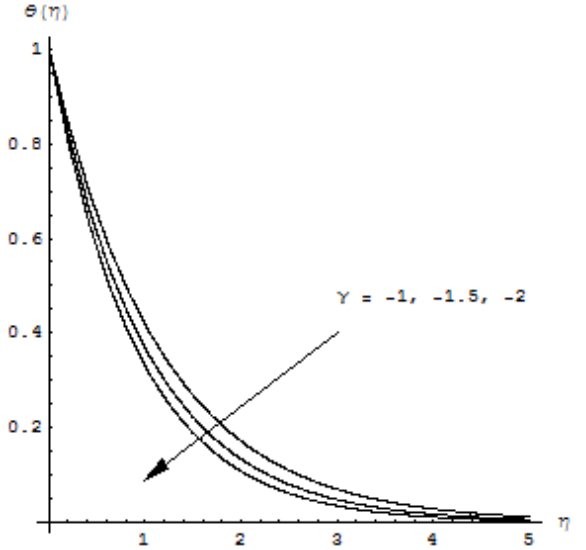

Figure 5(a): Variation of temperature corresponding to first solution for several values of γ with s = 2, M = 0.9, Pr = 1, R = 0.7, $\lambda = 0.1$ and p = 1.

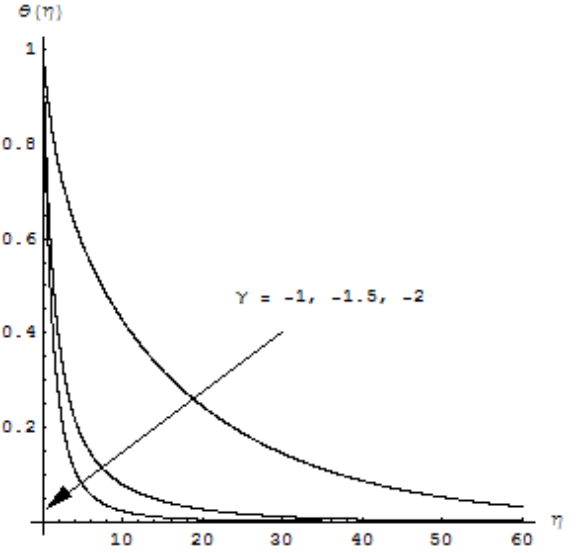

Figure 5(b): Temperature profiles corresponding to second solution for several values of γ when s = 2, M = 0.9, Pr = 1, R = 0.7, $\lambda = 0.1$ and p = 1.

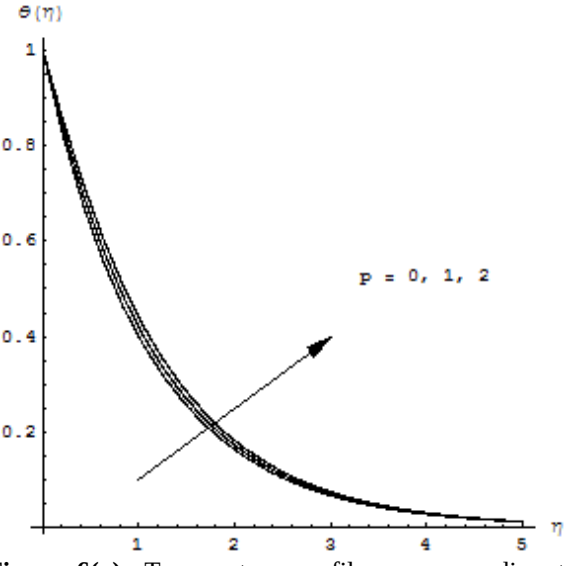

Figure 6(a): Temperature profiles corresponding to first solution for several values of p when s = 2, M = 0.9, Pr = 1, γ = - 1, $\lambda = 0.1$ and R = 0.7.

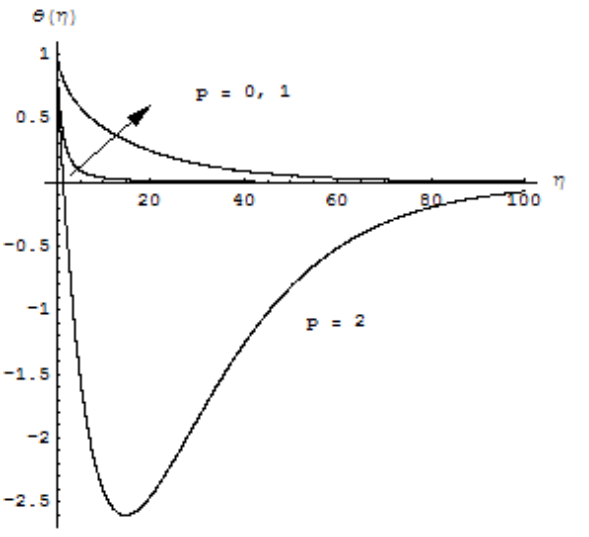

Figure 6(b): Variation of temperature corresponding to second solution for several values of p with s = 2, M = 0.9, Pr = 1, γ = - 1, $\lambda = 0.1$ and R = 0.7.

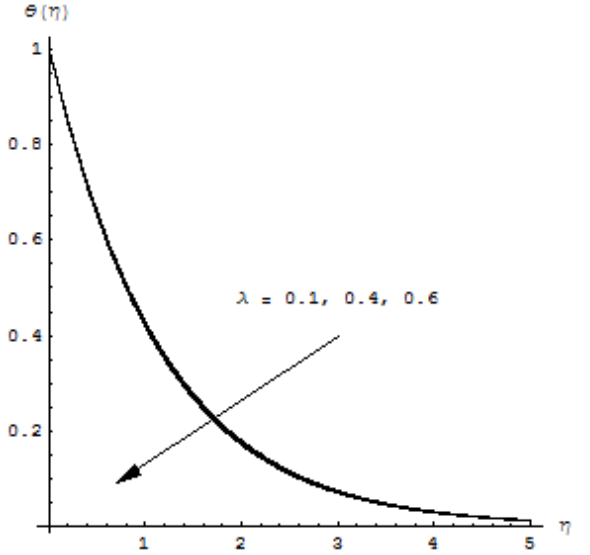

Figure 7(a): Variation of temperature corresponding to first solution for several values of λ with M = 0.6, s = 2, R = 0.7, Pr = 1, γ = - 1, and p = 1.

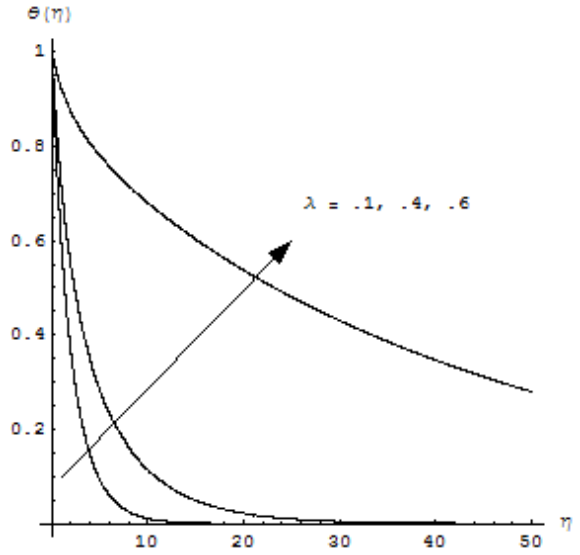

Figure 7(b): Temperature profiles corresponding to second solution for several values of λ when M = 0.6, s = 2, R = 0.7, Pr = 1, γ = - 1, and p = 1.

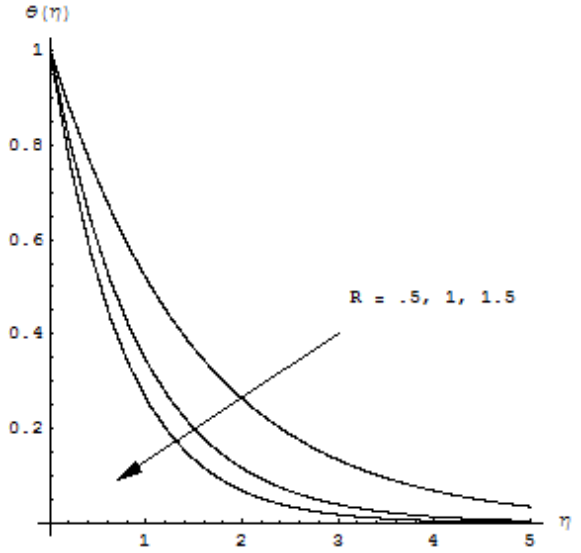

Figure 8: Variation of temperature corresponding to first solution for several values of R with s = 3, M = 0.5, Pr = 1, γ = 0.1, $\lambda = 0.1$ and p = 1.

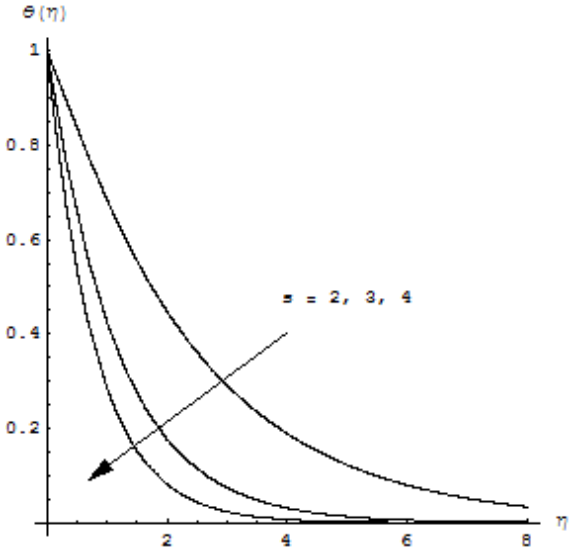

Figure 10: Variation of temperature corresponding to first solution for several values of s with M = 0.9, Pr = 1, R = 0.7, γ = 0.1, $\lambda = 0.1$ and p = 1.

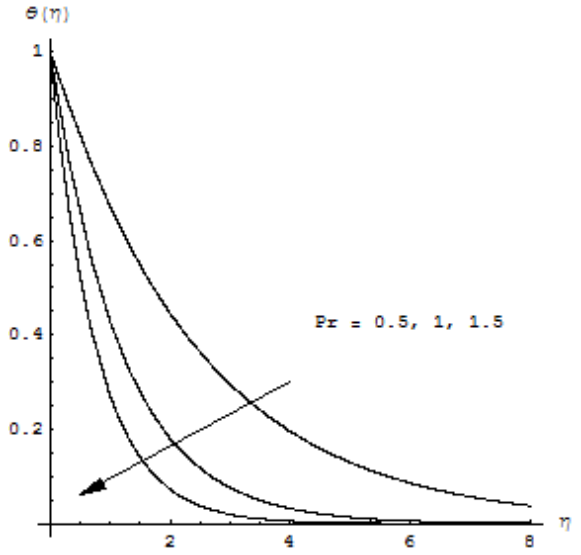

Figure 9: Temperature profiles corresponding to first solution for several values of Pr with s = 3, M = 0.5, R = 0.7, γ = 0.1, $\lambda = 0.1$ and p = 1.

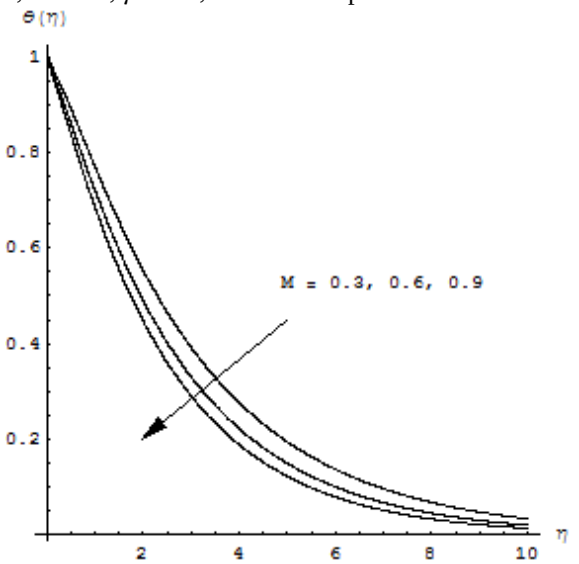

Figure 11: Temperature profiles corresponding to first solution for several values of M when s = 2, p = 1, Pr = 1, γ = 0.1, $\lambda = 0.1$ and R = 0.7.

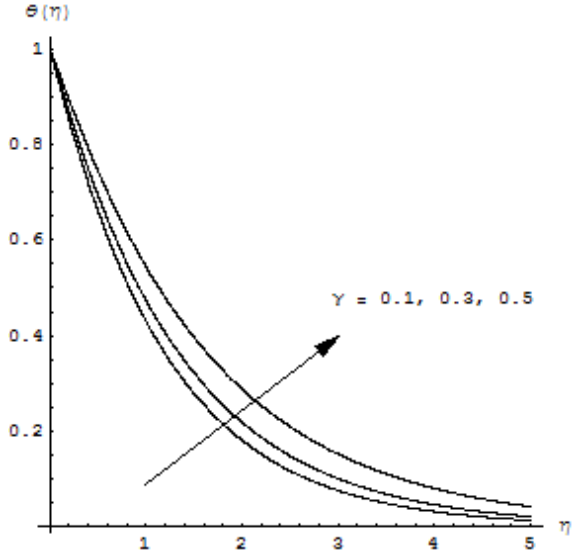

Figure 12: Temperature profiles corresponding to first solution for several values of γ with s = 3, R = 0.7, Pr = 1, M = 0.5, $\lambda = 0.1$ and p = 1.

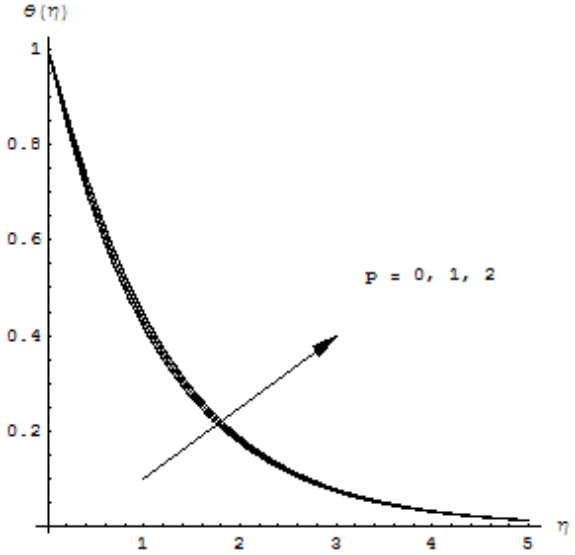

Figure 13: Temperature profiles corresponding to first solution for several values of p with M = 0.5, s = 3, R = 0.7, Pr = 1, $\gamma = 0.1$, $\lambda = 0.1$.

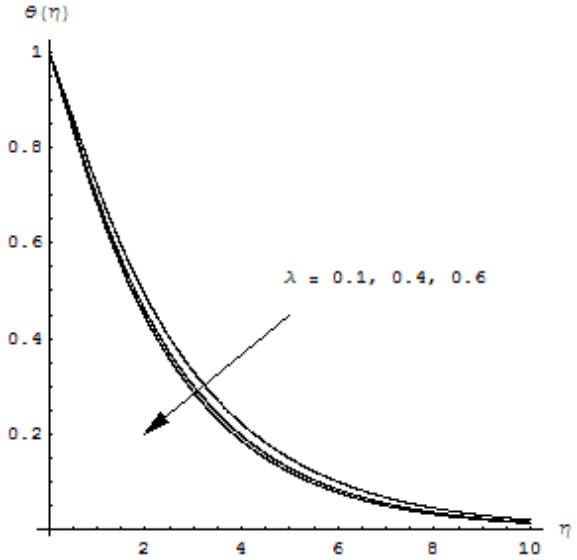

Figure 14: Variation of temperature corresponding to first solution for several values of λ with R = 0.7, M = 0.6, s = 2, Pr = 1, $\gamma = 0.1$, $\lambda = 0.1$ and p = 1.

Source of support: Nil, Conflict of interest: None Declared